Evaluation of autoconversion and accretion enhancement factors in general circulation model warm-rain parameterizations using ground-based measurements at the Azores

Peng Wu[1], *Baike Xi[1], Xiquan Dong[1], and Zhibo Zhang[2]

[1] Department of Hydrology and Atmospheric Sciences, The University of Arizona, Tucson, Arizona, USA

[2] Physics Department, The University of Maryland, Baltimore County, Maryland, USA

Submitted to Atmospheric Chemistry and Physics (November 28, 2018)

Keywords: MBL clouds, enhancement factors, autoconversion and accretion parameterizations

* Corresponding author address: Dr. Baike Xi, Department of Hydrology and Atmospheric Sciences, University of Arizona, 1133 E. James E. Rogers Way, Tucson, AZ 85721-0011. baike@email.arizona.edu; Phone: 520-626-8945

Abstract

A great challenge in climate modelling is how to parametrize sub-grid cloud processes, such as autoconversion and accretion in warm rain formation. In this study, we use ground-based observations and retrievals over the Azores to investigate the so-called enhancement factors, E_{auto} and E_{accr}, which are often used in climate models to account for the influence of sub-grid variances of cloud and precipitation water on the autoconversion and accretion processes. E_{auto} and E_{accr} are computed for different equivalent model grid sizes. The calculated E_{auto} values increase from 1.96 (30 km) to 3.2 (180 km), and the calculated E_{accr} values increase from 1.53 (30 km) to 1.76 (180 km). Comparing the prescribed enhancement factors in Morrison and Gettleman (2008, MG08) to the observed ones, we found that a higher E_{auto} (3.2) at small grids and lower E_{accr} (1.07) are used in MG08, which might explain why most of the GCMs produce too frequent precipitation events but with too light precipitation intensity. The ratios of rain to cloud water mixing ratio at E_{accr}=1.07 and E_{accr}=2.0 are 0.063 and 0.142, respectively, from observations, further suggesting that the prescribed value of E_{accr}=1.07 used in MG08 is too small to simulate precipitation intensity correctly. Both E_{auto} and E_{accr} increase when the boundary layer becomes less stable, and the values are larger in precipitating clouds (CLWP>75 gm^{-2}) than those in nonprecipiting clouds (CLWP<75 gm^{-2}). Therefore, the selection of E_{auto} and E_{accr} values in GCMs should be regime- and resolution- dependent.

1. Introduction

Due to their vast areal coverage (Warren et al., 1986, 1988; Hahn and Warren, 2007) and strong radiative cooling effect (Hartmann et al., 1992; Chen et al., 2000), small changes in the coverage or thickness of marine boundary layer (MBL) clouds could change the radiative energy budget significantly (Hartmann and Short, 1980; Randall et al., 1984) or even offset the radiative effects produced by increasing greenhouse gases (Slingo, 1990). The lifetime of MBL clouds remains an issue in climate models (Yoo and Li, 2012; Jiang et al., 2012; Yoo et al., 2013; Stanfield et al., 2014) and represents one of the largest uncertainties in predicting future climate (Wielicki et al., 1995; Houghton et al., 2001; Bony and Dufresne, 2005).

MBL clouds frequently produce precipitation, mostly in the form of drizzle (Austin et al., 1995; Wood, 2005a; Leon et al., 2008; Wood, 2012). A significant amount of drizzle evaporates before reaching the surface, for example, about ~76% over the Azores region in Northeast Atlantic (Wu et al., 2015), which provides a water vapour source for MBL clouds. Due to their pristine environment and their proximity to the surface, MBL clouds and precipitation are especially sensitive to aerosol perturbations (Platnick and Twomey, 1994). Thus, accurate prediction of precipitation is essential in simulating the global energy budget and in constraining aerosol indirect effects in climate projections.

Due to the coarse spatial resolutions of the general circulation model (GCM) grid, many cloud processes cannot be adequately resolved and must be parameterized. For example, warm

rain parameterizations in most GCMs treat the condensed water as either cloud or rain from the collision-coalescence process that is partitioned into autoconversion and accretion sub-processes in model parameterizations (Kessler, 1969; Tripoli and Cotton, 1980; Beheng, 1994; Khairoutdinov and Kogan, 2000; Liu and Daum, 2004). Autoconversion represents the process of drizzle drops being formed through the self-collection of cloud droplets and accretion represents the process where rain drops grow by collecting cloud droplets. Autoconversion mainly accounts for precipitation initiation while accretion primarily contributes to precipitation intensity. Autoconversion is often parameterized as functions of cloud droplet number concentration (N_c) and cloud water mixing ratio (q_c), while accretion depends on both cloud and rain water mixing ratios (q_c and q_r) (Kessler, 1969; Tripoli and Cotton, 1980; Beheng, 1994; Khairoutdinov and Kogan, 2000; Liu and Daum, 2004; Wood, 2005b). The majority of previous studies suggested that these two processes can be represented by power law functions of cloud and precipitation properties (See section 2 for details).

In conventional GCMs, the lack of information on the sub-grid variances of cloud and precipitation leads to the unavoidable use of the grid-mean quantities ($\overline{N_c}$, $\overline{q_c}$, and $\overline{q_r}$, where henceforth overbar denotes grid mean) in calculating autoconversion and accretion rates. MBL cloud liquid water path (CLWP) distributions are often positively skewed (Wood and Hartmann, 2006; Dong et al., 2014a and 2014b), that is, the mean value is greater than the mode value. Thus, the mean value only represents a relatively small portion of samples. Also,

due to the nonlinear nature of the relationships, the two processes depend significantly on the sub-grid variability and co-variability of cloud and precipitation microphysical properties (Weber and Quass, 2012; Boutle et al., 2014). In some GCMs, sub-grid scale variability is often ignored or hard-coded using constants to represent the variabilities under all meteorological conditions and across the entire globe (Pincus and Klein, 2000; Morrison and Gettleman, 2008; Lebsock et al., 2013). This could lead to systematic errors in precipitation rate simulations (Wood et al., 2002; Larson et al., 2011; Lebsock et al., 2013; Boutle et al., 2014; Song et al., 2018), where GCMs are found to produce too frequent but too light precipitation compared to observations (Zhang et al., 2002; Jess, 2010; Stephens et al., 2010; Nam and Quaas, 2012; Song et al., 2018). The bias is found to be smaller when using a probability density function (PDF) of cloud water to represent the sub-grid scale variability in autoconversion parameterization (Beheng, 1994; Zhang et al., 2002; Jess, 2010), or more complexly, by integrating the autoconversion rate over a joint PDF of liquid water potential temperature, and total water mixing ratio (Cheng and Xu, 2009).

Process rate enhancement factors (E) are introduced when considering sub-grid scale variability in parameterizing grid-mean processes and they should be parameterized as functions of the PDFs of cloud and precipitation properties within a grid box (Morrison and Gettleman, 2008; Lebsock et al., 2013; Boutle et al., 2014). However, these values in some GCM parameterization schemes are prescribed as constants regardless of surface or

meteorological conditions (Xie and Zhang, 2015). Boutle et al. (2014) used aircraft in situ measurements and remote sensing techniques to develop a parameterization for cloud and rain, in which they not only consider the sub-grid variabilities under different grid scales, but also consider the variation of cloud and rain fractions. The parameterization was found to reduce the precipitation estimation bias significantly. Hill et al. (2015) modified this parameterization and developed a regime and cloud type dependent sub-grid parameterization, which was implemented to the Met Office Unified Model by Walters et al. (2017) who found that the radiation bias is reduced when using the modified parameterization. Using ground-based observations and retrievals, Xie and Zhang (2015) proposed a scale-aware cloud inhomogeneity parameterization that they applied to the Community Earth System Model (CESM) and found that it can recognize spatial scales without manual tuning and can be applied to the entire globe. The inhomogeneity parameter is essential in calculating enhancement factors since they affect the conversion rate from cloud to rain liquid. Xie and Zhang (2015), however, did not evaluate the validity of CESM simulations from their parameterization; the effect of N_c variability or the effect of covariance of cloud and rain on the accretion process was not assessed. Most recently, Zhang et al. (2018) derived the sub-grid distribution of CLWP and N_c from the MODIS cloud product. They also studied the implication of sub-grid cloud property variations for the simulation of autoconversion, in particular the enhancement factor, in GCMs. For the first time, the enhancement factor due to the sub-grid variation of N_c was

derived from satellite observation, and results reveal several regions downwind of biomass burning aerosols (e.g., Gulf of Guinea, East Coast of South Africa), air pollution (i.e., Eastern China Sea), and active volcanos (e.g., Kilauea Hawaii and Ambae Vanuatu), where the enhancement factor due to N_c is comparable, or even larger than that due to CLWP. However, one limitation of Zhang et al. (2018) is the use of passive remote sensing data only, which cannot distinguish cloud and rain water.

Dong et al. (2014a and 2014b) and Wu et al. (2015) reported MBL cloud and rain properties over the Azores and provided the possibility of calculating the enhancement factors using ground-based observations and retrievals. In this study, a joint retrieval method to estimate q_c and q_r profiles is proposed based on existing studies (Appendix A). Most of the calculations and analyses in this study are based on the Morrison and Gettleman (2008, MG08 hereafter) scheme. The enhancement factors in several other schemes are also discussed and compared with the observational results and the approach in this study can be repeated for other microphysics schemes in GCMs. This manuscript is organized as follows: section 2 includes a summary of the mathematical formulas from previous studies that can be used to calculate enhancement factors. Ground-based observations and retrievals are introduced in Section 3. Section 4 presents results and discussions, followed by summary and conclusions in Section 5. The retrieval method used in this study is in Appendix A.

2. Mathematical Background

Autoconversion and accretion rates in GCMs are usually parameterized as power law equations (Tripoli and Cotton, 1980; Beheng, 1994; Khairoutdinov and Kogan, 2000; Liu and Daum, 2004):

$$\left(\frac{\partial q_r}{\partial t}\right)_{auto} = A\overline{q_c}^{a1}\overline{N_c}^{a2}, \quad (1)$$

$$\left(\frac{\partial q_r}{\partial t}\right)_{accr} = B(\overline{q_c}\overline{q_r})^b, \quad (2)$$

where A, $a1$, $a2$, B, and b are coefficients in different schemes listed in Table 1. The $\overline{q_c}$, $\overline{q_r}$, and $\overline{N_c}$ are grid-mean cloud water mixing ratio, rain water mixing ratio, and droplet number concentration, respectively. Because it is widely used in model parameterizations, the detailed results from Khairoutdinov and Kogan (2000) parameterization that has been used in MG08 scheme will be shown in Section 4 while a summary will be given for other schemes.

Ideally, the covariance between physical quantities should be considered in the calculation of both processes. However, $\overline{q_c}$ and $\overline{N_c}$ in Eq. (1) are arguably not independently retrieved in our retrieval method, which will be introduced in this section and Appendix A. Thus we only assess the individual roles of q_c and N_c sub-grid variations in determining the autoconversion rate. q_c and q_r, on the other hand, are retrieved from two independent algorithms as shown in Dong et al. (2014a and 2014b), Wu et al. (2015) and Appendix A. The effect of the covariance of q_c and q_r on accretion rate will be assessed.

At the sub-grid scale, the PDFs of q_c and N_c are assumed to follow a gamma distribution based on observational studies of optical depth in MBL clouds (Barker et al., 1996; Pincus et al., 1999; Wood and Hartmann, 2006):

$$P(x) = \frac{\alpha^{\nu}}{\Gamma(\nu)} x^{\nu-1} e^{-\alpha x}\,, \tag{3}$$

where x represents q_c or N_c with grid-mean quantity $\overline{q_c}$ or $\overline{N_c}$, represented by μ, $\alpha = \nu/\mu$ is the scale parameter, σ^2 is the relative variance of x (= variance divided by μ^2), $\nu = 1/\sigma^2$ is the shape parameter. ν is an indicator of cloud field homogeneity, with large values representing homogeneous and small values indicating inhomogeneous cloud fields.

By integrating autoconversion rate, Eq. (1), over the grid-mean rate, Eq. (3), with respect to sub-grid scale variation of q_c and N_c, the autoconversion rate can be expressed as:

$$\left(\frac{\partial q_r}{\partial t}\right)_{auto} = A\mu_{q_c}^{a1}\mu_{N_c}^{a2}\frac{\Gamma(\nu+a)}{\Gamma(\nu)\nu^a}, \tag{4}$$

where a = $a1$ or $a2$. Comparing Eq. (4) to Eq. (1), the autoconversion enhancement factor (E_{auto}) can be given with respect to q_c and N_c:

$$E_{auto} = \frac{\Gamma(\nu+a)}{\Gamma(\nu)\nu^a}\,. \tag{5}$$

In addition to fitting the distributions of q_c and N_c, we also tried two other methods to calculate E_{auto}. The first is to integrate Eq. (1) over the actual PDFs from observed or retrieved parameters and the second is to fit a lognormal distribution for sub-grid variability as has been done in other studies (e.g., Lebsock et al., 2013; Larson and Griffin, 2013). It is found that all

three methods provide similar results. In this study, we use a gamma distribution that is consistent with MG08. Also note that, in the calculation of E_{auto} from $\overline{N_c}$, the negative exponent (-1.79) may cause singularity problems in Eq. (5). When this situation occurs, we perform direct calculations by integrating the PDF of $\overline{N_c}$ rather than using Eq. (5).

To account for the covariance of microphysical quantities in a model grid, it is difficult to apply bivariate gamma distribution due to its complex nature. In this study, the bivariate lognormal distribution of q_c and q_r is used (Lebsock et al., 2013; Boutle et al., 2014) and can be written as:

$$P(\overline{q_c},\ \overline{q_r}) = \frac{1}{2\pi\overline{q_c}\,\overline{q_r}\sigma_{q_c}\sigma_{q_r}\sqrt{1-\rho^2}} exp\left\{-\frac{1}{2}\frac{1}{1-\rho^2}\left[\left(\frac{ln\overline{q_c}-\mu_{q_c}}{\sigma_{q_c}}\right)^2 - 2\rho\left(\frac{ln\overline{q_c}-\mu_{q_c}}{\sigma_{q_c}}\right)\left(\frac{ln\overline{q_r}-\mu_{q_r}}{\sigma_{q_r}}\right) + \left(\frac{ln\overline{q_r}-\mu_{q_r}}{\sigma_{q_r}}\right)^2\right]\right\}, \quad (6)$$

where σ is standard deviation and ρ is the correlation coefficient of q_c and q_r.

Similarly, by integrating the accretion rate in Eq. (2) from Eq. (6), we get the accretion enhancement factor (E_{accr}) of:

$$E_{accr} = \left(1+\frac{1}{\nu_{q_c}}\right)^{\frac{1.15^2-1.15}{2}}\left(1+\frac{1}{\nu_{q_r}}\right)^{\frac{1.15^2-1.15}{2}} \exp(\rho 1.15^2\sqrt{\ln\left(1+\frac{1}{\nu_{q_c}}\right)\ln(1+\frac{1}{\nu_{q_r}})}). \quad (7)$$

3. Ground-based observations and retrievals

The datasets used in this study were collected at the Department of Energy (DOE) Atmospheric Radiation Measurement (ARM) Mobile Facility (AMF), which was deployed on the northern coast of Graciosa Island (39.09°N, 28.03°W) from June 2009 to December 2010 (for more details, please refer to Rémillard et al., 2012; Dong et al., 2014a and Wood et al., 2015). The detailed operational status of the remote sensing instruments on AMF is summarized in Figure 1 of Rémillard et al. (2012) and discussed in Wood et al. (2015). The ARM Eastern North Atlantic (ENA) site was established on the same island in 2013 and provides long-term continuous observations.

The cloud-top heights (Z_{top}) were determined from the W-band ARM cloud radar (WACR) reflectivity and only single-layered and overcast low-level clouds with $Z_{top} \leq 3$ km were selected (the detailed selection criteria can be found in Dong et al., 2014a and 2014b). Cloud-base heights (Z_{base}) were detected by a laser ceilometer (CEIL) and the cloud thickness was simply the difference between cloud top and base heights. The cloud liquid water path (CLWP) was retrieved from microwave radiometer (MWR) brightness temperatures measured at 23.8 and 31.4 GHz using a statistical retrieval method with an uncertainty of 20 g m^{-2} for CLWP < 200 g m^{-2}, and 10% for CLWP > 200 g m^{-2} (Liljegren et al., 2001; Dong et al., 2000). Precipitating status is identified through a combination of WACR reflectivity and Z_{base}. As in Wu et al. (2015), we labelled the status of a specific time as "precipitating" if the WACR

reflectivity below the cloud base exceeds -37 dBZ. Note the differences of the reflectivity thresholds used here and in other studies. For example, -15 dBZ in Sauvageot and Omar (1987), -17 dBZ in Frisch et al. (1995), -19 to -16 dBZ in Wang and Geerts (2003) and -30 dBZ or lower in Kollias et al. (2011). The threshold used in this study is set at the cloud base rather than for the entire cloud layer as in the abovementioned studies. The -37 dBZ threshold is a statistical value from WACR observations at the Azores presented by Wu et al. (2015, Figure 2a), in which it is found that using a higher threshold will miss a significant number of drizzling events especially the clouds with virga.

The ARM merged sounding data have a 1-min temporal and 20-m vertical resolution below 3 km (Troyan, 2012). In this study, the merged sounding profiles are averaged to 5-min resolution. Pressure and temperature profiles are used to calculate air density (ρ_{air}) profiles and to infer adiabatic cloud water content.

Cloud droplet number concentration (N_c) is retrieved using the methods presented in Dong et al. (1998, 2014a and 2014b) and are assumed to be constant with height. Vertical profiles of cloud and rain water content (CLWC and RLWC) are retrieved by combining WACR reflectivity, CEIL attenuated backscatter and by assuming adiabatic growth of cloud water. A detailed description is presented in Appendix A with the results from a selected case. The CLWC and RLWC values are transformed to q_c and q_r by dividing by air density (e.g., $q_c(z) = CLWC(z)/\rho_{air}(z)$).

The estimated uncertainties for the retrieved q_c and q_r are 30% and 18%, respectively (see Appendix A). We used the estimated uncertainties of q_r and q_c as inputs of Eqs. (4) and (7) to assess the uncertainties of E_{auto} and E_{accr}. For instance, $(1 \pm 0.3)q_c$ are used in Eq. (4) and the mean differences are then used as the uncertainty of E_{auto}. The same method is used to estimate the uncertainty for E_{accr}.

The autoconversion and accretion parameterizations dominate at different levels in a cloud layer. Autoconversion dominates around cloud top where drizzle drops form by the self-collection of cloud droplets and accretion is dominant at middle and lower parts of the cloud where rain drops grow by collecting cloud droplets. In accordance with the physical processes, we estimate autoconversion and accretion rates at different levels of a cloud layer in this study. The averaged q_c within the top five range gates (~215 m thick) are used to calculate E_{auto}. To calculate E_{accr}, we use the averaged q_c and q_r within five range gates around the maximum radar reflectivity. If the maximum radar reflectivity appears at the cloud base, then five range gates above the cloud base are used.

The ARM merged sounding data are also used to calculate lower tropospheric stability ($LTS = \theta_{700\ hPa} - \theta_{1000\ hPa}$), which is used to infer the boundary layer stability. In this study, unstable and stable boundary layers are defined as LTS less than 13.5 K and greater than 18 K, respectively, and an environment with an LTS between 13.5 K and 18 K is defined as mid-stable (Wang et al. 2012; Bai et al. 2018). Enhancement factors in different boundary layers

241 are summarized in Section 4.2 and may be used as reference for model simulations. Further,
242 two regimes are classified: CLWP greater than 75 g m^{-2} as precipitating and CLWP less than
243 75 g m^{-2} as nonprecipitating (Rémillard et al., 2012).

244 To evaluate the dependence of autoconversion and accretion rates on sub-grid variabilities
245 for different model spatial resolutions, an average wind speed within a cloud layer was
246 extracted from merged sounding and used in sampling observations over certain periods to
247 mimic different grid sizes in GCMs. For example, two hours of observations correspond to a
248 72-km horizontal equivalent grid box if mean horizontal in-cloud wind speed is 10 $m\ s^{-1}$ and if
249 the wind speed is 5 $m\ s^{-1}$, four hours of observations are needed to mimic the same horizontal
250 equivalent grid. We used six horizontal equivalent grid sizes (30-, 60-, 90-, 120-, 150-, and
251 180-km) and mainly show the results from 60-km and 180-km horizontal equivalent grid sizes
252 in Section 4. For convenience, we use 'equivalent size' to imply 'horizontal equivalent grid
253 size' from now on.

254 **4. Results and discussions**

255 In this section, we first show the data and methods using a selected case, followed by
256 statistical analysis based on 19 months of data and multiple time-intervals.

257 **4.1 Case study**

258 The selected case occurred on July 27, 2010 (Figure 1a) at the Azores. This case was
259 characterized by a long period of non-precipitating or light drizzling cloud development

(00:00-14:00 UTC) before intense drizzle occurred (14:00-20:00 UTC). Wu et al. (2017) studied this case in detail to demonstrate the effect of wind shear on drizzle initiation. Here, we choose two periods corresponding to a 180-km equivalent size and having similar mean q_c near cloud top: 0.28 g kg^{-1} for period c and 0.26 g kg^{-1} for period d, but with different distributions (Figures 1c and 1d). The PDFs of q_c are then fitted using gamma distributions to get shape parameters (ν) as shown in Figures 1c and 1d. Smaller ν is usually associated with a more inhomogeneous cloud field, which allows more rapid drizzle production and more efficient liquid transformation from cloud to rain (Xie and Zhang, 2015) in regions that satisfy precipitation criteria, which is usually controlled using a threshold q_r, droplet size or relative humidity (Kessler, 1969; Liu and Daum, 2004). The period d has a wider q_c distribution than the period c, resulting in a smaller ν and thus larger E_{auto}. Using the fitted ν, the E_{auto} from q_c calculated from Eq. (5) for the period d is larger than for period c (1.80 vs. 1.33). The E_{auto} values for the d and c can also be calculated from N_c using the same procedure as q_c with a similar result (2.1 vs. 1.51). The E_{accr} values for periods d and c can be calculated from the covariance of q_c and q_r and Eq. (7). Not surprisingly, period d has larger E_{accr} than period c. The combination of larger E_{auto} and E_{accr} in period d contributes to rapid drizzle production and high rain rate as seen from WACR reflectivity and q_r in Figure A1.

It is important to understand the physical meaning of enhancement factors in precipitation parameterization. For example, if we assume two scenarios for q_c with a model grid having the

same mean values but different distributions: (1) The distribution is extremely homogeneous, there will be no sub-grid variability because the cloud has the same chance to precipitate and the enhancement factors would be unity (this is true for arbitrary grid-mean q_c amount as well). (2) The cloud field gets more and more inhomogeneous with a broad range of q_c within the model grid box, which results in a greater enhancement factor and increases the possibility of precipitation. That is, a large enhancement factor can make the part of the cloud with higher q_c within the grid box more efficient in generating precipitation, rather than the entire model grid.

Using the LWP retrieved from the Moderate Resolution Imaging Spectroradiometer (MODIS) as an indicator of cloud inhomogeneity, Wood and Hartmann (2006) found that when clouds become more inhomogeneous, cloud fraction decreases, and open cells become dominant, accompanied by stronger drizzle (Comstock et al., 2007). The relationship between reduced homogeneity and stronger precipitation intensity found in this study is similar to the findings in other studies (e.g., Wood and Hartmann, 2006, Comstock et., 2007, Barker et al., 1996; Pincus et al., 1999).

It is clear that q_c and N_c in Figure 1b are correlated with each other. In addition to their natural relationships, q_c and N_c in our retrieval method are also correlated (Dong et al., 2014a and 2014b). Thus, the effect of q_c and N_c covariance on E_{auto} is not included in this study. In Figures 1c and 1d, the results are calculated using an equivalent size of 180-km for the selected case on 27 July 2010. In Section 4.2, we will use these approaches to calculate their statistical

results for multiple equivalent sizes using the 19-month ARM ground-based observations and retrievals.

4.2 Statistical result

For a specific equivalent size, e.g. 60-km, we estimate the shape parameter (ν) and calculate E_{auto} through Eqns. (5) and (7). The PDFs of E_{auto} for both 60-km and 180-km equivalent sizes are shown in Figures 2a-2d. The distributions of E_{auto} values calculated from q_c with 60-km and 180-km equivalent sizes (Figures 2a and 2b) are different to each other (2.79 vs. 3.3). The calculated E_{auto} values range from 1 to 10, and most are less than 4. The average value for the 60-km equivalent size (2.79) is smaller than that for the 180-km equivalent size (3.2), indicating a possible dependence of E_{auto} on model grid size. Because drizzle-sized drops are primarily formed by autoconversion, we investigate the relationship between E_{auto} and precipitation frequency, which is defined as the average percentage of drizzling occurrence based on radar reflectivity below cloud base. Given the average LWP at Azores from Dong et al. (2014b, 109-140 g m^{-2}), the precipitation frequency (black lines in Figures 2a and 2b) agrees well with those from Kubar et al. (2009, 0.1-0.7 from their Figure 11). The precipitation frequency within each bin shows an increasing trend for E_{auto} from 0 to 4-6, then oscillates when $E_{auto} > 6$, indicating that in the precipitation initiation process, E_{auto} keeps increasing to a certain value (~6) until the precipitation frequency reaches a near-steady state. Higher precipitation frequency does not

316 necessarily result in larger E_{auto} values but instead may produce more drizzle-sized drops from
317 autoconversion process when the cloud is precipitating.

318 The PDFs of E_{auto} calculated from N_c also share similar patterns of positive skewness and
319 peaks at ~1.5-2.0 for the 60-km and 180-km equivalent sizes (Figures 2c and 2d). Although the
320 average values are close to their q_c counterparts (2.54 vs. 2.79 for 60-km and 3.45 vs. 3.2 for
321 180-km), the difference in E_{auto} between 60-km and 180-km equivalent sizes becomes large.
322 The precipitation frequencies within each bin are nearly constant or decrease slightly, which
323 are different to their q_c counterparts shown in Figures 2a and 2b. This suggests complicated
324 effects of droplet number concentration on precipitation initiation and warrants more
325 exploration of aerosol-cloud-precipitation interactions. As mentioned in Section 2, q_c and N_c
326 are also fitted using lognormal distributions to calculate E_{auto}. The results are close to those in
327 Figure 2 (not shown here) with average values of 3.28 and 3.84, respectively, for 60-km and
328 180-km equivalent sizes. Because the E_{auto} values calculated from q_c and N_c are close to each
329 other, we will focus on analyzing the results from q_c only for simplicity and clarity. The effect
330 of q_c and N_c covariance, as stated in Section 4.1, is not presented in this study due to the intrinsic
331 correlation in the retrieval (Dong et al., 2014a and 2014b and Appendix A of this study).

332 The covariance of q_c and q_r is included in calculating E_{accr} and the results are shown in
333 Figures 2e and 2f. The calculated E_{accr} values range from 1 to 4 with mean values of 1.62 and
334 1.76 for 60-km and 180-km equivalent sizes, respectively. These two mean values are much

greater than the prescribed value used in MG08 (1.07). Since accretion is dominant in the middle and lower parts of the cloud where rain drops sediment and continue to grow by collecting cloud droplets, we superimpose the ratio of q_r to q_c within each bin (black lines in Figures 2e and 2f) to represent the portion of rain water in the cloud layer. In both panels, the ratios are less than 15%, which means that q_r can be one order of magnitude smaller than q_c. The differences in magnitude are consistent with previous CloudSat and aircraft results (e.g., Boutle et al., 2014). This ratio increases from E_{accr}=0 to ~2, and then decreases, suggesting that the conversion efficiency cannot be infinitely increase with E_{accr} under available cloud water. The ratio of q_r to q_c increases from E_{accr}=1.07 (0.063) to E_{accr}=2.0 (0.142), indicating that the fraction of rain water in total liquid water using the prescribed E_{accr} is too low. This ratio could be increased significantly using a large E_{accr} value, therefore increasing precipitation intensity in the models. This further suggests that the prescribed value of E_{accr}=1.07 used in MG08 is too small to correctly simulate precipitation intensity in the models. Therefore, similar to the conclusions in Lebsock et al. (2013) and Boutle et al. (2014), we suggest increasing E_{accr} from 1.07 to 1.5-2.0 in GCMs.

To illustrate the impact of using prescribed enhancement factors, autoconversion and accretion rates are calculated using the prescribed values (e.g., 3.2 for E_{auto} and 1.07 for E_{accr}, MG08; Xie and Zhang, 2015) and the newly calculated ones in Figure 2 that use observations and retrievals. Figure 3 shows the joint density of autoconversion (Figures 3a and 3b) and

accretion rates (Figures 3c and 3d) from observations (x-axis) and model parameterizations (y-axis) for 60-km and 180-km equivalent sizes. Despite the spread, the peaks in the joint density of autoconversion rate appear slightly above the one-to-one line especially for the 60-km equivalent size, suggesting that cloud droplets in the model are more easily to be converted into drizzle/rain drops than in the observations. On the other hand, the peaks in the accretion rate appear slightly below the one-to-one line, which indicates that simulated precipitation intensities are lower than observed ones. The magnitudes of the two rates are consistent with Khairoutdinov and Kogan (2000), Liu and Daum (2004), and Wood (2005b).

Compared to the observations, the precipitation in GCMs occurs at higher frequencies with lower intensities, which might explain why the total precipitation amounts are close to surface measurements over an entire grid box. This 'promising' result, however, fails to simulate precipitation on the right scale and cannot capture the correct rain water amount, thus providing limited information in estimating rain water evaporation and air-sea energy exchange.

Clouds in an unstable boundary layer have a better chance of getting moisture supply from the surface by upward motion than clouds in a stable boundary layer. Precipitation frequencies are thus different in these two boundary layer regimes. For example, clouds in a relatively unstable boundary layer produce drizzle more easily than those in a stable boundary layer. Given the same boundary layer conditions, CLWP is an important factor in determining the precipitation status of clouds. At the Azores, precipitating clouds are more likely to have

CLWP greater than 75 g m^{-2} than their nonprecipitating counterparts (Rémillard et al., 2012). To further investigate what conditions and parameters can significantly influence the enhancement factors, we classify low-level clouds according to their boundary layer conditions and CLWPs.

The averaged E_{auto} and E_{accr} values for each category are listed in Table 2. Both E_{auto} and E_{accr} increase when the boundary layer becomes less stable, and these values become larger in precipitating clouds (CLWP>75 gm^{-2}) than those in nonprecipiting clouds (CLWP<75 gm^{-2}). In model parameterizations, the autoconversion process only occurs when q_c or cloud droplet size reaches a certain threshold (e.g., Kessler, 1969 and Liu and Daum, 2004). Thus, it will not affect model simulations if a valid E_{auto} is assigned to Eq. (1) in a nonprecipitating cloud. The E_{auto} values in both stable and mid-stable boundary layer conditions are smaller than the prescribed value of 3.2, while the values in unstable boundary layers are significantly larger than 3.2, regardless of whether they are precipitating. All E_{accr} values are greater than the constant of 1.07. The E_{auto} values in Table 2 range from 2.32 to 6.94 and the E_{accr} values vary from 1.42 to 1.86, depending on different boundary layer conditions and CLWPs. Therefore, as suggested by Hill et al. (2015), the selection of E_{auto} and E_{accr} values in GCMs should be regime-dependent.

To properly parameterize sub-grid variabilities, the approaches of Hill et al. (2015) and Walters et al. (2017) can be adopted. To use MG08 and other parameterizations in GCMs as

listed in Table 1, proper adjustments can be made according to the model grid size, boundary layer conditions, and precipitating status. As stated in the methodology, we used a variety of equivalent sizes. Figure 4 demonstrates the dependence of both enhancement factors on different model grid sizes. The E_{auto} values (red line) increase from 1.97 at an equivalent size of 30 km to 3.15 at an equivalent size of 120 km, which are 38.4% and 2% percent lower than the prescribed value (3.2, upper dashed line). After that, the E_{auto} values remain relatively constant at ~3.18 when the equivalent model size is 180 km, which is close to the prescribed value of 3.2 used in MG08. This result indicates that the prescribed value in MG08 is appropriate for large grid sizes in GCMs. The E_{accr} values (blue line) increase from 1.53 at an equivalent size of 30 km to 1.76 at an equivalent size of 180 km, increases of 43% and 64%, respectively, larger than the prescribed value (1.07, lower dashed line). The shaded areas represent the uncertainties in E_{auto} and E_{accr} associated with the uncertainties in the retrieved q_c and q_r. When equivalent size increases, the uncertainties decrease slightly. The prescribed E_{auto} is close to the upper boundary of uncertainties except for the 30-km equivalent size, while the prescribed E_{accr} is significantly lower than the lower boundary.

It is noted that E_{auto} and E_{accr} depart from their prescribed values in opposite directions as the equivalent size increases. For models with finer resolutions (e.g., 30-km), both E_{auto} and E_{accr} are significantly different from the prescribed values, which can partially explain the issue of 'too frequent' and 'too light' precipitation. Under both conditions, the accuracy of

411 precipitation estimation is degraded. For models with coarser resolutions (e.g., 180-km), the
412 average E_{auto} is exactly 3.2 while E_{accr} is much larger than 1.07 when compared to finer
413 resolution simulations. In such situations, the simulated precipitation will be dominated by the
414 'too light' problem, in addition to regime-dependent (Table 2) and as in Xie and Zhang (2015),
415 E_{auto} and E_{accr} should also be scale-dependent.

416 Also note that the location of ground-based observations and retrievals used in this study is
417 on the remote ocean where the MBL clouds mainly form in a relatively stable boundary layer
418 and are characterized by high precipitation frequency. Even in such environments, however,
419 GCMs overestimate the precipitation frequency (Ahlgrimm and Forbes, 2014).

420 To further investigate how enhancement factors affect precipitation simulations, we use
421 E_{auto} as a fixed value of 3.2 in Eq. (4), and then calculate the q_c needed for models to reach the
422 same autoconversion rate as observations. The q_c differences between models and observations
423 are then calculated, which represent the q_c adjustment in models to achieve a realistic
424 autoconversion rate in the simulations. Similar to Figure 1, the PDFs of q_c differences (model
425 – observation) are plotted in Figures 5a and 5b for 60-km and 180-km equivalent sizes. Figure
426 5c shows the average percentages of model q_c adjustments for different equivalent sizes. The
427 mode and average values for the 30-km equivalent size is negative, suggesting that models
428 need to simulate lower q_c in general to get reasonable autoconversion rates. Lower q_c values
429 are usually associated with smaller E_{auto} values that induce lower simulated precipitation

frequency. On average, the percentage of q_c adjustments decreases with increasing equivalent size. For example, the adjustments for finer resolutions (e.g., 30-60 km) can be ~20% of the q_c, whereas adjustments in coarse resolution models (e.g., 120 – 180 km) are relatively small because the prescribed E_{auto} (=3.2) is close to the observed ones (Figure 4), and when equivalent size is 180-km, no adjustment is needed. The adjustment method presented in Figure 5, however, may change cloud water substantially and may cause a variety of subsequent issues, such as altering cloud radiative effects and disrupting the hydrological cycle. The assessment in Figure 5 only provides a reference to the equivalent effect on cloud water by using the prescribed E_{auto} value as compared to those from observations.

All above discussions are based on the prescribed E_{auto} and E_{accr} values (3.2 and 1.07) in MG08, whereas there are quite a few parameterizations that have been published so far. In this study, we list E_{auto} and E_{accr} for three other widely used parameterization schemes in Table 3, which are given only for 60-km and 180-km equivalent sizes. The values of the exponent in each scheme directly affect the values of the enhancement factors. For example, the scheme in Beheng (1994) has the highest degree of nonlinearity and hence has the largest enhancement factors. The scheme in Liu and Daum (2004) is very similar to the scheme in Khairoutdinov and Kogan (2000) because both schemes have a physically realistic dependence on cloud water content and number concentration (Wood, 2005b). For a detailed overview and discussion of various existing parameterizations, please refer to Liu and Daum (2004), Liu et al. (2006a), Liu

et al. (2004b), Wood (2005b) and Michibata and Takemura (2015). A physical based autoconversion parameterization was developed by Lee and Baik (2017) in which the scheme was derived by solving the stochastic collection equation with an approximated collection kernel that is constructed using the terminal velocity of cloud droplets and the collision efficiency obtained from a particle trajectory model. Due to the greatly increased complexity of their equation, we do not attempt to calculate E_{auto} here but it should be examined in future studies due to the physically appealing Lee and Baik (2017) scheme.

5. Summary

To better understand the influence of sub-grid cloud variations on the warm-rain process simulations in GCMs, we investigated the warm-rain parameterizations of autoconversion (E_{auto}) and accretion (E_{accr}) enhancement factors in MG08. These two factors represent the effects of sub-grid cloud and precipitation variabilities when parameterizing autoconversion and accretion rates as functions of grid-mean quantities. E_{auto} and E_{accr} are prescribed as 3.2 and 1.07, respectively, in the widely used MG08 scheme. To assess the dependence of the two parameters on sub-grid scale variabilities, we used ground-based observations and retrievals collected at the DOE ARM Azores site to reconstruct the two enhancement factors in different equivalent sizes.

From the retrieved q_c and q_r profiles, the averaged q_c within the top five range gates are used to calculate E_{auto} and the averaged q_c and q_r within five range gates around maximum reflectivity are used to calculate E_{accr}. The calculated E_{auto} values from observations and retrievals increase from 1.96 at an equivalent size of 30 km to 3.18 at an equivalent size of 150 km. These values are 38% and 0.625% lower than the prescribed value of 3.2. The prescribed value in MG08 represents well the large grid sizes in GCMs (e.g., 180^2 km^2 grid). On the other hand, the E_{accr} values increase from 1.53 at an equivalent size of 30 km to 1.76 at an equivalent size of 180 km, which are 43% and 64% higher than the prescribed value (1.07). The higher E_{auto} and lower E_{accr} prescribed in GCMs help to explain the issue of too frequent precipitation events with too light precipitation intensity. The ratios of rain to cloud liquid water increase with increasing E_{accr} from 0 to 2, and then decrease thereafter and the values at E_{accr}=1.07 and E_{accr}=2.0 are 0.063 and 0.142, further underscoring that the prescribed value of E_{accr}=1.07 is too small to simulate correct precipitation intensity in models.

To further investigate what conditions and parameters can significantly influence the enhancement factors, we classified low-level clouds according to their boundary layer conditions and CLWPs. Both E_{auto} and E_{accr} increase when the boundary layer conditions become less stable, and the values are larger in precipitating clouds (CLWP>75 gm^{-2}) than those in nonprecipiting clouds (CLWP<75 gm^{-2}). The E_{auto} values in both stable and mid-stable boundary layer conditions are smaller than the prescribed value of 3.2, while those in unstable

boundary layers conditions are significantly larger than 3.2 regardless of whether or not the cloud is precipitating (Table 2). All E_{accr} values are greater than the prescribed value of 1.07. Therefore, the selection of E_{auto} and E_{accr} values in GCMs should be regime-dependent, which also has been suggested by Hill et al. (2015) and Walters et al. (2017).

This study, however, did not include the effect of uncertainties in GCM simulated cloud and precipitation properties on sub-grid scale variations. For example, we did not consider the behavior of the two enhancement factors under different aerosol regimes, a condition which may affect the precipitation formation process. The effect of aerosol-cloud-precipitation-interactions on cloud and precipitation sub-grid variabilities may be of comparable importance to meteorological regimes and precipitation status and deserves a further study. Other than the large-scale dynamics, e.g., LTS in this study, upward/downward motion in sub-grid scale may also modify cloud and precipitation development and affect the calculations of enhancement factors. The investigation of the dependence of E_{auto} and E_{accr} on aerosol type and concentration as well as on vertical velocity would be a natural extension and complement of the current study. In addition, other factors may also affect precipitation frequency and intensity even under the same aerosol regimes and even if the clouds have similar cloud water contents. Wind shear, for example as presented in Wu et al. (2017), is an external variable that can affect precipitation formation. Further studies are needed to evaluate the role of the covariance of q_c

and N_c at sub-grid scales on E_{auto}, which is beyond the scope of this study and requires independent retrieval techniques.

Appendix A: Joint cloud and rain LWC profile estimation

If a time step is identified as non-precipitating, the cloud liquid water content (CLWC) profile is retrieved using Frisch et al. (1995) and Dong et al. (1998, 2014a and 2014b). The retrieved CLWC is proportional to radar reflectivity.

If a time step is identified as precipitatinging (maximum reflectivity below cloud base exceeds -37 dBZ), CLWC profile is first inferred from temperature and pressure in merged sounding by assuming adiabatic growth. Marine stratocumulus clouds are close to adiabatic (Albrecht et a. 1990) which assists cloud property retrievals (e.g., Rémillard et al., 2013). In this study, we use the information from rain properties near cloud base to further constrain the adiabatic CLWC ($CLWC_{adiabatic}$).

Adopting the method of O'Connor et al. (2005), Wu et al. (2015) retrieved rain properties below cloud base (CB) for the same period as in this study. In Wu et al. (2015), rain drop size (median diameter, D_0), shape parameter (μ), and normalized rain droplet number concentration (N_W) are retrieved for the assumed rain particle size distribution (PSD):

$$n_r(D) = N_W f(\mu) \left(\frac{D}{D_0}\right)^{\mu} \exp\left[-\frac{(3.67+\mu)D}{D_0}\right] \quad \text{(A1)}$$

To infer rain properties above cloud base, we adopt the assumption in Fielding et al. (2015) that N_W increases from below CB to within the cloud. This assumption is consistent with the *in situ* measurement in Wood (2005a). Similar to Fielding et al. (2015), we use constant N_W within cloud if the vertical gradient of N_W is negative below CB. The μ within cloud is treated as constant and is taken as the average value from four range gates below CB. Another assumption in the retrieval is that the evaporation of rain drops is negligible from one range gate above CB to one range gate below CB thus we assume rain drop size is the same at the range gate below and above CB.

With the above information, we can calculate the reflectivity contributed by rain at the first range gate above CB ($Z_r(1)$) and the cloud reflectivity ($Z_c(1)$) is then $Z_c(1) = Z(1) - Z_r(1)$, where $Z(1)$ is the WACR measured reflectivity at the first range gate above CB. Using the cloud droplet number concentration (N_c) from Dong et al. (2014a and 2014b), CLWC at the first range gate above CB can be calculated through

$$Z_c(1) = 2^6 \int_0^\infty n_c(r) r^6 dr = \frac{36}{\pi^2 \rho_w^2} \frac{CLWC(1)_{reflectivity}{}^2}{N_c} \exp(9\sigma_x^2) \quad \text{(A2.1)}$$

$$CLWC(1)_{reflectivity} = \sqrt{\frac{Z_c(1)\, \pi^2 \rho_w^2\, N_c}{36 \exp(9\sigma_x^2)}} \quad \text{(A2.2)}$$

Where ρ_w is liquid water density $n_c(r)$ is lognormal distribution of cloud PSD with logarithmic width σ_x. Geoffroy et al. (2010) suggested that σ_x increases with the length scale and Witte et al. (2018) showed that σ_x is also dependent on the choice of instrumentation. The

variations of σ_x should be reflected in the retrieval by using different σ_x values with time. However, no aircraft measurements were available during CAP-MBL to provide σ_x over the Azores region. The inclusion of solving σ_x in the retrieval adds another degree of freedom to the equations and complicates the problem considerably. In this study, σ_x is set to a constant value of 0.38 from Miles et al. (2000), which is a statistical value from aircraft measurements in marine low-level clouds.

We then compare the $CLWC_{adiabatic}$ and the one calculated from $CLWC_{reflectivity}$ at the first range gate above CB. A scale parameter (s) is defined as $s = \frac{CLWC_{reflectivity}(1)}{CLWC_{adiabatic}(1)}$ and the entire profile of $CLWC_{adiabatic}$ is multiplied by s to correct the bias from cloud sub-adiabaticity. The reflectivity profile from the cloud is then calculated from Eq. (A2.1) using the updated $CLWC_{adiabatic}$ and the remaining reflectivity profile from the WACR observation is regarded as the rain contribution. Rain particle size can then be calculated given that N_W and μ are known and rain liquid water content (RLWC) can be estimated.

There are two constrains used in the retrieval. One is that the summation of cloud and rain liquid water path (CLWP and RLWP) must be equal to the LWP from the microwave radiometer observation. Another is that rain drop size (D_0) near cloud top must be equal or greater than 50 μm and if D_0 is less than 50 μm, we decrease N_W for the entire rain profile within cloud and repeat the calculation until the 50 μm criterion is satisfied.

It is difficult to quantitatively estimate the retrieval uncertainties without aircraft in situ measurements. For the proposed retrieval method, 18% should be used as uncertainty for RLWC from rain properties in Wu et al. (2015) and 30% for CLWC from cloud properties in Dong et al. (2014a and 2014b). The actual uncertainty depends on the accuracy of the merged sounding data, the sensitivity of WACR near cloud base and the effect of entrainment on cloud adiabaticity during precipitating. A recent aircraft field campaign, the Aerosol and Cloud Experiments in Eastern North Atlantic (ACE-ENA), was conducted during 2017-2018 with a total of 39 flights over the Azores, near the ARM ENA site on Graciosa Island. These aircraft in situ measurements will be used to validate the ground-based retrievals and quantitatively estimate their uncertainties in the future.

Figure A1 shows an example of the retrieval results. The merged sounding, ceilometer, microwave radiometer, WACR and ceilometer are used in the retrieval. Whenever one or more instruments are not reliable, that time step is skipped, and this results in the gaps in the CLWC and RLWC as shown in Figures A1(b) and A1(c). When the cloud is classified as nonprecipitating, no RLWC will be retrieved. Using air density (ρ_{air}) profiles calculated from temperature and pressure in merged sounding, mixing ratio (q) can be calculated from LWC using $q(z) = LWC(z)/\rho_{air}(z)$.

Acknowledgements

The ground-based measurements were obtained from the Atmospheric Radiation Measurement (ARM) Program sponsored by the U.S. Department of Energy (DOE) Office of Energy Research, Office of Health and Environmental Research, and Environmental Sciences Division. The data can be downloaded from http://www.archive.arm.gov/. This research was supported by the DOE CESM project under grant DE-SC0014641 at the University of Arizona through subaward from University of Maryland at Baltimore County, and the NSF project under grant AGS-1700728 at University of Arizona. The authors thank Dr. Yangang Liu at Brookhaven National Laboratory for insightful comments and Ms. Casey E. Oswant at the University of Arizona for proof reading the manuscript. The three anonymous reviewers are acknowledged for constructive comments and suggestions, which helped to improve the manuscript. We appreciate the comments and corrections from the CO Editor, Dr. Graham Feingold.

References

Ahlgrimm, M., and Forbes, R.: Improving the Representation of Low Clouds and Drizzle in the ECMWF Model Based on ARM Observations from the Azores, J. Clim., doi: 10.1175/MWR-D-13-00153.1, 2014.

Albrecht, B., Fairall, C., Thomson, D., White, A., Snider, J., and Schubert, W.: Surface-based remote-sensing of the observed and the adiabatic liquid water-content of stratocumulus clouds, Geophys. Res. Lett., 17, 89–92, doi:10.1029/Gl017i001p00089, 1990.

Austin, P., Wang, Y., Kujala, V., and Pincus, R.: Precipitation in Stratocumulus Clouds: Observational and Modeling Results, J. Atmos. Sci., 52, 2329–2352, doi:10.1175/1520-0469(1995)052<2329:PISCOA>2.0.CO;2, 1995.

Bai, H., Gong, C., Wang, M., Zhang, Z., and L'Ecuyer, T.: Estimating precipitation susceptibility in warm marine clouds using multi-sensor aerosol and cloud products from A-Train satellites, Atmos. Chem. Phys., 18, 1763-1783, https://doi.org/10.5194/acp-18-1763-2018, 2018.

Barker H. W., Wiellicki B.A., Parker L.: A parameterization for computing grid-averaged solar fluxes for inhomogeneous marine boundary layer clouds. Part II: Validation using satellite data. J. Atmos. Sci. 53: 2304–2316, 1996.

Beheng, K. D.: A parameterization of warm cloud microphysical conversion processes, Atmos. Res., 33, 193-206, 1994.

Bony, S., and Dufresne, J.-L.: Marine boundary layer clouds at the heart of tropical cloud feedback uncertainties in climate models, Geophys. Res. Lett., 32, L20806, doi:10.1029/2005GL023851, 2005.

Boutle, I. A., Abel, S. J., Hill, P. G., and Morcrette, C. J.: Spatial variability of liquid cloud and rain: Observations and microphysical effects. Quart. J. Roy. Meteor. Soc., 140, 583–594, doi:10.1002/qj.2140, 2014.

Chen, T., Rossow, W. B., and Zhang, Y.: Radiative Effects of Cloud-Type Variations, J. Clim., 13, 264–286, 2000.

Cheng, A., and Xu. K.-M.: A PDF-based microphysics parameterization for simulation of drizzling boundary layer clouds, J. Atmos. Sci., 66, 2317–2334, doi:10.1175/2009JAS2944.1, 2009.

Comstock, K. K., Yuter, S. E., Wood, R., and Bretherton, C. S.: The Three-Dimensional Structure and Kinematics of Drizzling Stratocumulus, Mon. Weather Rev., 135, 3767–3784, doi:10.1175/2007MWR1944.1, 2007.

Dong X., Ackerman, T. P., and Clothiaux, E. E.: Parameterizations of Microphysical and Radiative Properties of Boundary Layer Stratus from Ground-based measurements, J. Geophys. Res., 102, 31,681-31,393, 1998.

Dong, X., Minnis, P., Ackerman, T. P., Clothiaux, E. E., Mace, G. G., Long, C. N., and Liljegren, J. C.: A 25-month database of stratus cloud properties generated from ground-based measurements at the ARM SGP site, J. Geophys. Res., 105, 4529-4538, 2000.

Dong, X., Xi, B., Kennedy, A., Minnis, P. and Wood, R.: A 19-month Marine Aerosol-Cloud_Radiation Properties derived from DOE ARM AMF deployment at the Azores: Part I: Cloud Fraction and Single-layered MBL cloud Properties, J. Clim., 27, doi:10.1175/JCLI-D-13-00553.1, 2014a.

Dong, X., Xi, B., and Wu, P.: Investigation of Diurnal Variation of MBL Cloud Microphysical Properties at the Azores, J. Clim., 27, 8827-8835, 2014b.

Fielding, M. D., Chiu, J. C., Hogan, R. J., Feingold, G., Eloranta, E., O'Connor, E. J. and Cadeddu, M. P.: Joint retrievals of cloud and drizzle in marine boundary layer clouds using ground-based radar, lidar and zenith radiances. Atmospheric Measurement Techniques, 8. pp. 2663-2683. ISSN 1867-8548 doi: 10.5194/amt-8-2663-2015, 2015.

Frisch, A., Fairall, C., and Snider, J.: Measurement of stratus cloud and drizzle parameters in ASTEX with a Ka-band Doppler radar and a microwave radiometer, J. Atmos. Sci., 52, 2788–2799, 1995.

Geoffroy, O., Brenguier, J.-L., and Burnet, F.: Parametric representation of the cloud droplet spectra for LES warm bulk microphysical schemes, Atmos. Chem. Phys., 10, 4835-4848, https://doi.org/10.5194/acp-10-4835-2010, 2010.

644 Hahn, C. and Warren, S.: A gridded climatology of clouds over land (1971–96) and ocean
645 (1954–97) from surface observations worldwide, Numeric Data Package NDP-026E
646 ORNL/CDIAC-153, CDIAC, Department of Energy, Oak Ridge, Tennessee, 2007.
647 Hartmann, D. L., Ockert-Bell, M. E., and Michelsen, M. L.: The Effect of Cloud Type on
648 Earth's Energy Balance: Global Analysis, J. Climate, 5, 1281–1304,
649 https://doi.org/10.1175/15200442(1992)005<1281:TEOCTO>2.0.CO;2, 1992.
650 Hartmann, D. L. and Short, D. A.: On the use of earth radiation budget statistics for studies of
651 clouds and climate, J. Atmos. Sci., 37, 1233–1250, doi:10.1175/1520-
652 0469(1980)037<1233:OTUOER>2.0.CO;2, 1980.
653 Hill, P. G., Morcrette, C. J., and Boutle, I. A.: A regime-dependent parametrization of subgrid-
654 scale cloud water content variability, Q. J. R. Meteorol. Soc., 141, 1975–1986, 2015.
655 Houghton, J. T., Ding, Y., Griggs, D.J., Noguer, M., van der Linden, P.J., Dai, X., Maskell, K.,
656 and Johnson, C.A.: Climate Change: The Scientific Basis, Cambridge University Press,
657 881 pp, 2001.
658 Jess, S.: Impact of subgrid variability on large-scale precipitation formation in the climate
659 model ECHAM5, PhD thesis, Dep. of Environ. Syst. Sci., ETH Zurich, Zurich,
660 Switzerland, 2010.
661 Jiang, J., Su, H., Zhai, C., Perun, V. S., Del Genio, A., Nazarenko, L. S., Donner, L. J.,
662 Horowitz, Seman, L., Cole, C., J., Gettelman, A., Ringer, M. A., Rotstayn, L., Jeffrey, S.,
663 Wu, T., Brient, F., Dufresne, J-L., Kawai, H., Koshiro, T., Watanabe, M., LÉcuyer, T. S.,
664 Volodin, E. M., Iversen, Drange, T., H., Mesquita, M. D. S., Read, W. G., Waters, J. W.,
665 Tian, B., Teixeira, J., and Stephens, G. L.: Evaluation of cloud and water vapor simulations
666 in CMIP5 climate models using NASA ''A-train'' satellite observations, J. Geophys. Res.,
667 117, D14105, doi:10.1029/2011JD017237, 2012.

668 Kessler, E.: On the distribution and continuity of water substance in atmospheric circulations,
669 Met. Monograph 10, No. 32, American Meteorological Society, Boston, USA, 84 pp.,
670 1969.
671 Khairoutdinov, M. and Kogan, Y.: A New Cloud Physics Parameterization in a Large-Eddy
672 Simulation Model of Marine Stratocumulus, Mon. Wea. Rev.,128, 229-243, 2000.
673 Kollias, P., Szyrmer, W., Rémillard, J., and Luke, E.: Cloud radar Doppler spectra in drizzling
674 stratiform clouds:2. Observations and microphysical modeling of drizzle evolution, J.
675 Geophys. Res., 116, D13203, doi:10.1029/2010JD015238, 2011.
676 Kubar, T. L., Hartmann, D. L., and Wood, R.: Understanding the importance of microphysics
677 and macrophysics in marine low clouds, Part I: satellite observations. J. Atmos. Sci., 66,
678 2953-2972, doi: 10.1175/2009JAS3071.1, 2009.
679 Larson, V. E., Nielsen, B. J., Fan, J., and Ovchinnikov, M.: Parameterizing correlations
680 between hydrometeor species in mixed-phase Arctic clouds, J. Geophys. Res., 116,
681 D00T02, doi:10.1029/2010JD015570, 2011.
682 Larson, V. E., and Griffin, B. M.: Analytic upscaling of a local microphysics scheme. Part I:
683 Derivation. Quart. J. Roy. Meteor. Soc., 139, 46–57, 2013.
684 Lebsock, M. D., Morrison, H., and Gettelman, A.: Microphysical implications of cloud-
685 precipitation covariance derived from satellite remote sensing, J. Geophys. Res.-Atmos.,
686 118, 6521–6533, https://doi.org/10.1002/jgrd.50347, 2013.
687 Lee, H., and Baik, J.-J.: A physically based autoconversion parameterization. Journal of the
688 Atmospheric Sciences, 74, 1599–1616, 2017.
689 Leon, D. C., Wang, Z., and Liu, D.: Climatology of drizzle in marine boundary layer clouds
690 based on 1 year of data from CloudSat and Cloud-Aerosol Lidar and Infrared Pathfinder
691 Satellite Observations (CALIPSO), J. Geophys. Res., 113, D00A14,
692 doi:10.1029/2008JD009835, 2008.

693 Liljegren, J. C., Clothiaux, E. E., Mace, G. G., Kato, S., and Dong, X.: A new retrieval for
694 cloud liquid water path using a ground-based microwave radiometer and measurements of
695 cloud temperature, J. Geophys. Res., 106, 14,485-14,500, 2001.
696 Liu, Y. and Daum, P. H.: Parameterization of the autoconversion process, Part I: Analytical
697 formulation of the Kessler-type parameterizations, J. Atmos. Sci., 61, 1539–1548, 2004.
698 Liu, Y., Daum, P. H., and McGraw, R.: Parameterization of the autoconversion process. Part
699 II: Generalization of Sundqvist-type parameterizations, J. Atmos. Sci., 63, 1103–1109,
700 2006a.
701 Liu, Y., Daum, P. H., McGraw, R., Miller, M.: Generalized threshold function accounting for
702 effect of relative dispersion on threshold behavior of autoconversion process. Geophys.
703 Res. Lett., 33, L11804, 2006b.
704 Michibata, T., and Takemura, T.: Evaluation of autoconversion schemes in a single model
705 framework with satellite observations, J. Geophys. Res. Atmos., 120, 9570–9590,
706 doi:10.1002/2015JD023818, 2015.
707 Miles, N. L., Verlinde, J., and Clothiaux, E. E.: Cloud-droplet size distributions in low-level
708 stratiform clouds. J. Atmos. Sci., 57, 295–311, doi:10.1175/1520-0469(2000)057,
709 0295:CDSDIL.2.0.CO;2, 2000.
710 Morrison, H. and Gettelman, A.: A new two-moment bulk stratiform cloud microphysics
711 scheme in the Community Atmosphere Model, version 3 (CAM3). Part I: Description and
712 numerical tests, J. Climate, 21, 3642–3659, 2008.
713 Nam, C., and Quaas, J.: Evaluation of clouds and precipitation in the ECHAM5 general
714 circulation model using CALIPSO and CloudSat satellite data, J. Clim., 25, 4975–4992,
715 doi:10.1175/JCLI-D-11-00347.1, 2012.
716 O'Connor, E. J., Hogan, R. J., and Illingworth, A. J.: Retrieving stratocumulus drizzle
717 parameters using Doppler radar and lidar, J. of Applied Meteorol., 44, 14-27, 2005.

718 Platnick, S. and Twomey, S.: Determining the Susceptibility of Cloud Albedo to Changes in
719 Droplet Concentration with the Advanced Very High Resolution Radiometer, J. Appl.
720 Meteorol., 33, 334–347, 1994.
721 Pincus, R., McFarlane, S. A., and Klein, S. A.: Albedo bias and the horizontal variability of
722 clouds in subtropical marine boundary layers: Observations from ships and satellites, J.
723 Geophys. Res., 104, 6183–6191, doi:10.1029/1998JD200125, 1999.
724 Pincus, R., and Klein, S. A.: Unresolved spatial variability and microphysical process rates in
725 large-scale models. J. Geophys. Res., 105D, 27 059–27 065, 2000.
726 Randall, D. A., Coakley, J. A., Fairall, C. W., Knopfli, R. A., and Lenschow, D. H.: Outlook
727 for research on marine subtropical stratocumulus clouds. Bull. Amer. Meteor. Soc., 65,
728 1290–1301, 1984.
729 Rémillard, J., Kollias, P., Luke, E., and Wood, R.: Marine Boundary Layer Cloud Observations
730 in the Azores, J. Climate, 25, 7381–7398, doi: http://dx.doi.org/10.1175/JCLI-D-11-
731 00610.1, 2012.
732 Rémillard, J., Kollias, P., and Szyrmer, W.: Radar-radiometer re- trievals of cloud number
733 concentration and dispersion parameter in nondrizzling marine stratocumulus, Atmos.
734 Meas. Tech., 6, 1817–1828, doi:10.5194/amt-6-1817-2013, 2013.
735 Sauvageot, H., and Omar, J.: Radar reflectivity of cumulus clouds, J. Atmos. Oceanic Technol.,
736 4, 264–272, 1987.
737 Slingo, A.: Sensitivity of the Earth's radiation budget to changes in low clouds, Nature, 343,
738 49–51, https://doi.org/10.1038/343049a0, 1990.
739 Song, H., Zhang, Z., Ma, P.-L., Ghan, S. J., and Wang, M.: An Evaluation of Marine Boundary
740 Layer Cloud Property Simulations in the Community Atmosphere Model Using Satellite
741 Observations: Conventional Subgrid Parameterization versus CLUBB, J. Clim.,
742 doi:10.1175/JCLI-D-17-0277.1, 2018.

743 Stanfield, R., Dong, X., Xi, B., Gel Genio, A., Minnis, P., and Jiang, J.: Assessment of NASA
744 GISS CMIP5 and post CMIP5 Simulated Clouds and TOA Radiation Budgets Using
745 Satellite Observations: Part I: Cloud Fraction and Properties, J. Clim., doi:10.1175/JCLI-
746 D-13-00588.1, 2014.
747 Tripoli, G. J. and Cotton, W. R.: A numerical investigation of several factors contributing to
748 the observed variable intensity of deep convection over South Florida., J. Appl. Meteorol.,
749 19, 1037–1063, 1980.
750 Troyan, D.: Merged Sounding Value-Added Product, Tech. Rep., DOE/SC-ARM/TR-087,
751 2012.
752 Walters, D., Baran, A., Boutle, I., Brooks, M., Earnshaw, P., Edwards, J., Furtado, K., Hill, P.,
753 Lock, A., Manners, J., Morcrette, C., Mulcahy, J., Sanchez, C., Smith, C., Stratton, R.,
754 Tennant, W., Tomassini, L., van Weverberg, K., Vosper, S., Willett, M., Browse, J.,
755 Bushell, A., Dalvi, M., Essery, R., Gedney, N., Hardiman, S., Johnson, B., Johnson, C.,
756 Jones, A., Mann, G., Milton, S., Rumbold, H., Sellar, A., Ujiie, M., Whitall, M., Williams,
757 K. and Zerroukat, M. The Met Office Unified Model Global Atmosphere 7.0/7.1 and
758 JULES Global Land 7.0 configurations. Geosci. Model Dev., doi:10.5194/gmd-2017-291,
759 2017.
760 Wang, J., and Geerts, B.: Identifying drizzle within marine stratus with W-band radar
761 reflectivity, Atmos. Res., 69, 1–27, 2003.
762 Wang, M., Ghan, S., Liu, X., L'Ecuyer, T. S., Zhang, K., Morrison, H., Ovchinnikov, M.,
763 Easter, R., Marchand, R., Chand, D., Qian, Y., and Penner, J. E.: Constraining cloud
764 lifetime effects of aerosols using A-Train satellite observations, Geophys. Res. Lett., 39,
765 L15709, https://doi.org/10.1029/2012GL052204, 2012.
766 Warren, S. G., Hahn, C. J., London, J., Chervin, R. M., and Jenne, R.: Global distribution of
767 total cloud cover and cloud type amount over land, Tech. Rep. Tech. Note TN-317 STR,
768 NCAR, 1986.

769 Warren, S. G., Hahn, C. J., London, J., Chervin, R. M., and Jenne, R.: Global distribution of
770 total cloud cover and cloud type amount over land, Tech. Rep. Tech. Note TN-317 STR,
771 NCAR, 1988.
772 Weber, T., and Quaas, J.: Incorporating the subgrid-scale variability of clouds in the
773 autoconversion parameterization using a PDF-scheme, J. Adv. Model. Earth Syst., 4,
774 M11003, doi:10.1029/2012MS000156, 2012.
775 Wielicki, B. A., Cess, R. D., King, M. D., Randall, D. A., and Harrison, E. F.: Mission to planet
776 Earth: Role of clouds and radiation in climate, Bull. Amer. Meteor. Soc., 76, 2125–2153,
777 doi:10.1175/1520-0477(1995)076,2125:MTPERO.2.0.CO;2, 1995.
778 Witte, M. K., Yuan, T., Chuang, P. Y., Platnick, S., Meyer, K. G., Wind, G., and Jonsson, H.
779 H.: MODIS retrievals of cloud effective radius in marine stratocumulus exhibit no
780 significant bias. Geophysical Research Letters, 45, 10,656–10,664.
781 https://doi.org/10.1029/2018GL079325, 2018.
782 Wood, R., Field, P. R., and Cotton, W. R.: Autoconversion rate bias in stratiform boundary
783 layer cloud parameterization. Atmos. Res., 65, 109–128, 2002.
784 Wood, R.: Drizzle in stratiform boundary layer clouds. Part I: Vertical and horizontal structure,
785 J. Atmos. Sci., 62, 3011–3033, 2005a.
786 Wood, R.: Drizzle in stratiform boundary layer clouds. Part II: Microphysical aspects, J.
787 Atmos. Sci., 62, 3034–3050, 2005b.
788 Wood, R. and Hartmann, D.: Spatial variability of liquid water path in marine low cloud: The
789 importance of mesoscale cellular convection, J. Climate, 19, 1748–1764, 2006.
790 Wood, R.: Cancellation of aerosol indirect effects in marine stratocumulus through cloud
791 thinning. J. Atmos. Sci., 64, 2657–2669, 2007.
792 Wood, R.: Stratocumulus Clouds, Mon. Wea. Rev., 140, 2373–2423. doi:
793 http://dx.doi.org/10.1175/MWR-D-11-00121.1, 2012.

794 Wood, R., Wyant, M., Bretherton, C. S., Rémillard, J., Kollias, P., Fletcher, J., Stemmler, J.,
795 deSzoeke, S., Yuter, S., Miller, M., Mechem, D., Tselioudis, G., Chiu, C., Mann, J.,
796 O'Connor, E., Hogan, R., Dong, X., Miller, M., Ghate, V., Jefferson, A., Min, Q., Minnis,
797 P., Palinkonda, R., Albrecht, B., Luke, E., Hannay, C., Lin, Y.: Clouds, Aerosol, and
798 Precipitation in the Marine Boundary Layer: An ARM Mobile Facility Deployment, Bull.
799 Amer. Meteorol. Soc., doi: http://dx.doi.org/10.1175/BAMS-D-13-00180.1, 2015.
800 Wu, P., Dong, X. and Xi, B.: Marine boundary layer drizzle properties and their impact on
801 cloud property retrieval, Atmos. Meas. Tech., 8, 3555–3562. doi: 10.5194/amt-8-3555-
802 2015, 2015.
803 Wu, P., Dong, X., Xi, B., Liu, Y., Thieman, M., and Minnis, P.: Effects of environment forcing
804 on marine boundary layer cloud-drizzle processes, J. Geophys. Res. Atmos., 122, 4463–
805 4478, doi:10.1002/2016JD026326, 2017.
806 Xie, X., and Zhang, M.: Scale-aware parameterization of liquid cloud inhomogeneity and its
807 impact on simulated climate in CESM, J. Geophys. Res. Atmos., 120, 8359–8371,
808 doi:10.1002/2015JD023565, 2015.
809 Yoo, H., and Li, Z.: Evaluation of cloud properties in the NOAA/NCEP Global Forecast
810 System using multiple satellite products. Climate Dyn., 39, 2769–2787,
811 doi:10.1007/s00382-012-1430-0, 2012.
812 Yoo, H., and Li, Z., Hou, Y.-T., Lord, S., Weng, F., and Barker, H. W.: Diagnosis and testing
813 of low-level cloud parameterizations for the NCEP/GFS using satellite and ground-based
814 measurements. Climate Dyn., 41, 1595–1613, doi:10.1007/s00382-013-1884-8, 2013.
815 Zhang, J., Lohmann, U., and Lin, B.: A new statistically based autoconversion rate
816 parameterization for use in large-scale models. J. Geophys. Res., 107, 4750,
817 doi:10.1029/2001JD001484, 2002.
818 Zhang, Z., Song, H., Ma, P.-L., Larson, V., Wang, M., Dong, X., and Wang, J.: Subgrid
819 variations of cloud water and droplet number concentration over tropical oceans: satellite

820 observations and implications for warm rain simulation in climate models. Submitted to
821 Atmos. Chem. Phys., 2018.
822

Table 1. The parameters of autoconversion and accretion formulations for four parameterizations.

	A	$a1$	$a2$	B	b
Khairoutdinov and Kogan (2000)	1350	2.47	-1.79	67	1.15
Liu and Daum (2004)	$1.3 \times 10\beta_6^6$, where $\beta_6^6 = [(r_v + 3)/r_v]^2$, r_v is mean volume radius. modification was made by Wood (2005b)	3	-1	N/A	N/A
Tripoli and Cotton (1980)	3268	7/3	-1/3	1	1
Beheng (1994)	3×10^{34} for $N_c < 200$ cm^{-3} 9.9 for $N_c > 200$ cm^{-3}	4.7	-3.3	1	1

827 **Table 2. Autoconversion (left) and accretion (right) enhancement factors in different**
828 **boundary layer conditions (LTS > 18 K for stable, LTS < 13.5 K for unstable and LTS**
829 **within 13.5 and 18 K for mid-stable) and in different LWP regimes (LWP ≤ 75 g m^{-2} for**
830 **non-precipitating and LWP > 75 g m^{-2} for precipitating).**
831

	LWP ≤ 75 g m^{-2}	LWP > 75 g m^{-2}
LTS > 18 K	2.32/1.42	2.75/1.52
13.5 ≤ LTS ≤ 18K	2.61/1.47	3.07/1.68
LTS < 13.5 K	4.62/1.72	6.94/1.86

832

Table 3. Autoconversion and accretion enhancement factors (E_{auto} and E_{accr}) for the parameterizations in Table 1 except the Khairoutdinov and Kogan (2000) scheme. The values are averaged for 60-km and 180-km equivalent sizes.

	E_{auto}		E_{accr}	
	60-km	180-km	60-km	180-km
Liu and Daum (2004)	3.82	4.23	N/A	N/A
Tripoli and Cotton (1980)	2.46	2.69	1.47	1.56
Beheng (1994)	6.94	5.88	1.47	1.56

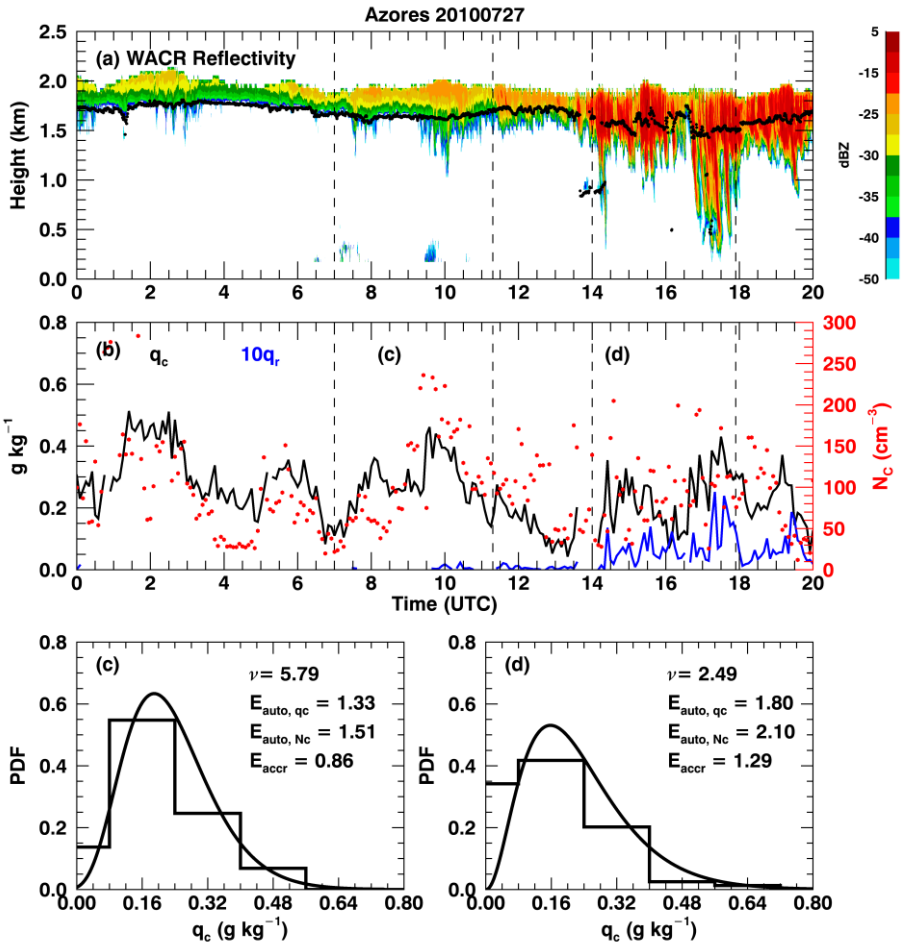

Figure 1. Observations and retrievals over the Azores on 27 July 2010. (a) W-band ARM cloud radar (WACR) reflectivity (contour) superimposed with cloud-base height (black dots). (b) Black line represents averaged cloud water mixing ratio (q_c) within the top five range gates, blue line represents averaged rain (×10) water mixing ratio within five range gates around maximum reflectivity, red dots are the retrieved cloud droplet number concentration (N_c). Dashed lines represent two periods that have 60 km equivalent sizes with similar $\overline{q_c}$ but different distributions as shown by step lines in (c) and (d). Curved lines in (c) and (d) are fitted gamma distributions with the corresponding shape parameter (ν) shown on the upper right. N_c distributions are not shown. The calculated autoconversion ($E_{auto, qc}$ from q_c and $E_{auto, Nc}$ from N_c) and accretion (E_{accr}) enhancement factors are also shown.

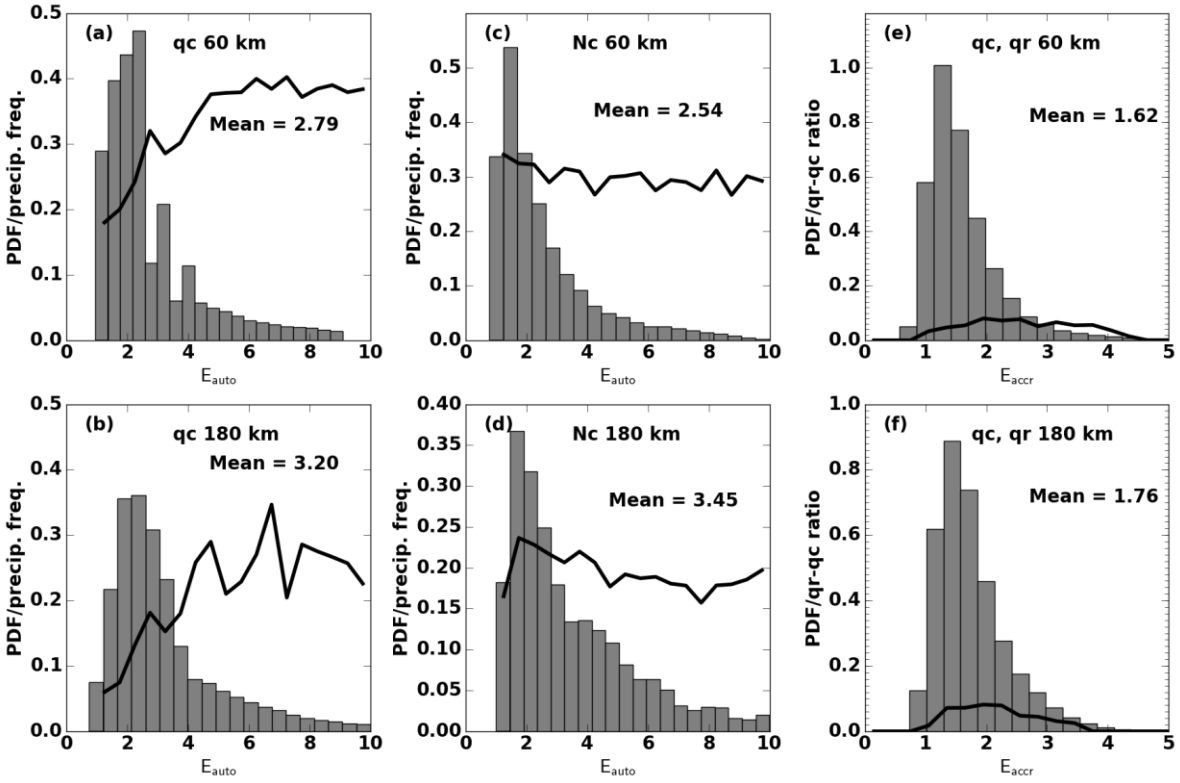

Figure 2. Probability density functions (PDFs) of autoconversion (a - d) and accretion (e - f) enhancement factors calculated from q_c (a-b), N_c (c-d), and the covariance of q_c and q_r (e-f). The two rows show the results from 60-km and 180-km equivalent sizes, respectively, with their average values. Black lines represent precipitation frequency in each bin in (a)-(d) and the ratio of layer-mean q_r to q_c in (e)-(f).

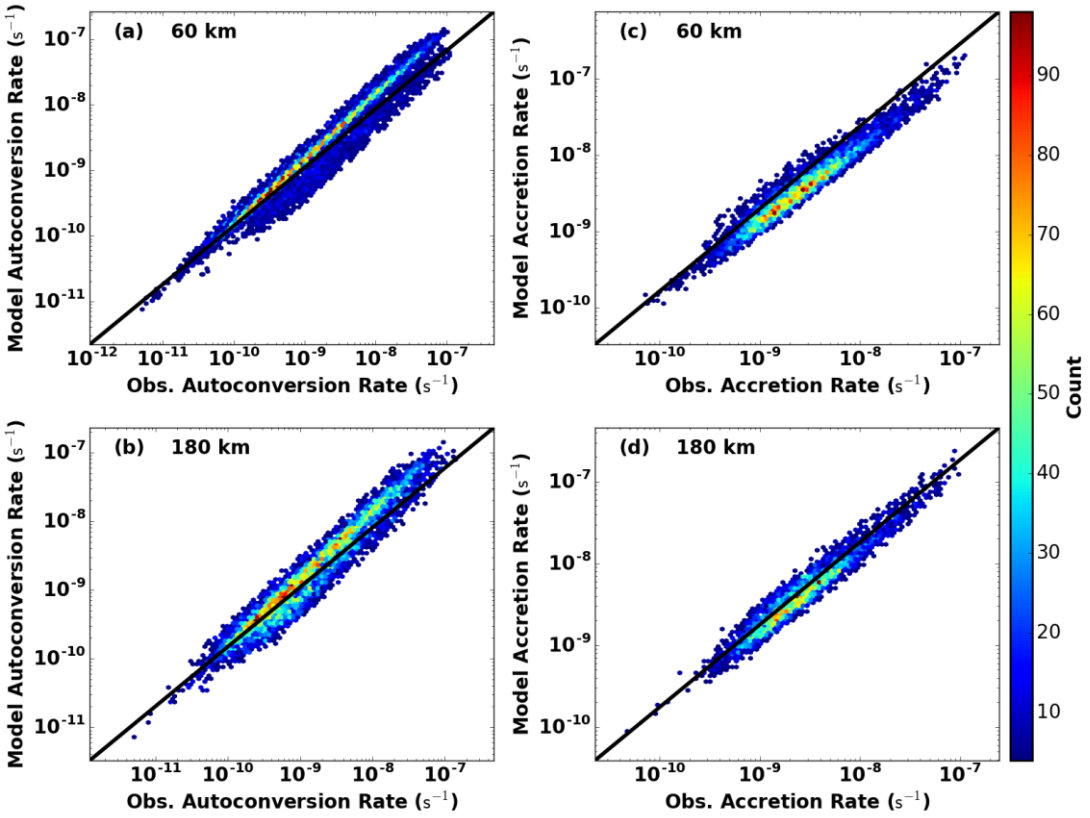

859

860 **Figure 3. Comparison of autoconversion (a-b) and accretion (c-d) rates derived from**
861 **observations (x-axis) and from model (y-axis). Results are for 60-km (a and c) and 180-**
862 **km model equivalent sizes. Colored dots represent joint number densities.**

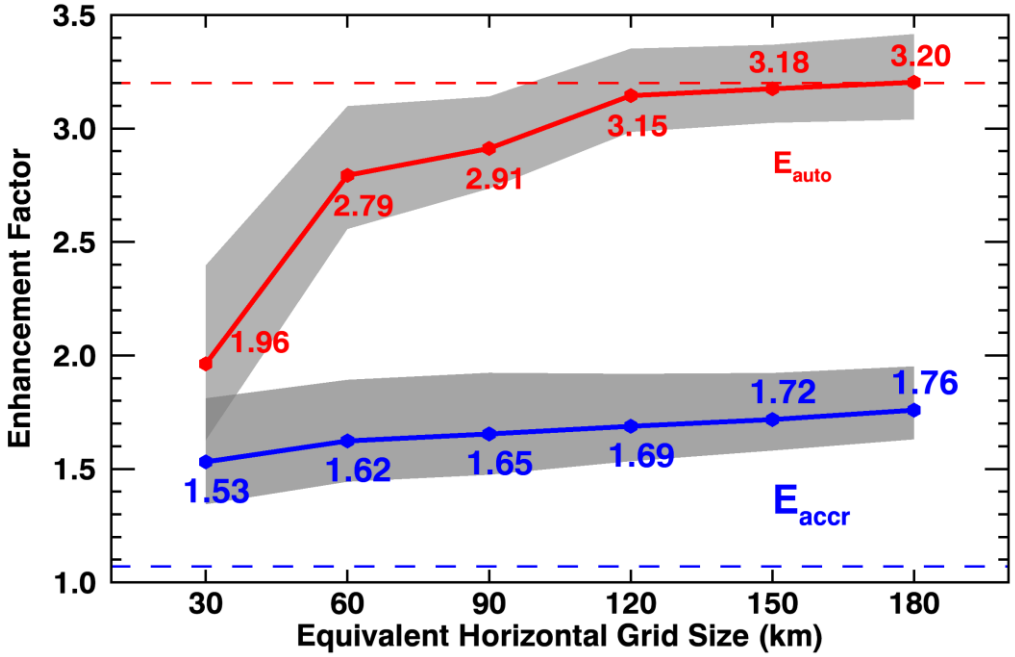

Figure 4. Autoconversion (red line) and accretion (blue line) enhancement factors as a function of equivalent sizes. The shaded areas are calculated by varying q_c and q_r within their retrieval uncertainties. The two dashed lines show the constant values of autoconversion (3.2) and accretion (1.07) enhancement factors prescribed in MG08.

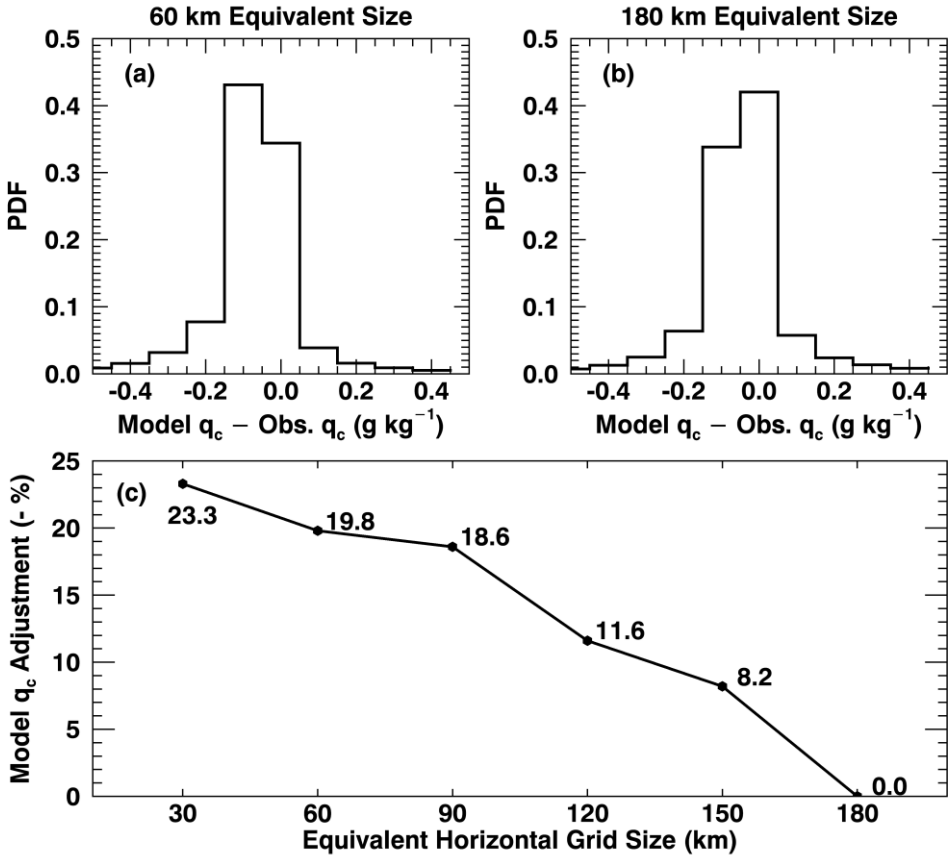

869

870 **Figure 5. q_c needed for models to adjust to reach the same autoconversion rate as**
871 **observations for (a) 60-km and (b) 180-km model equivalent sizes. Positive biases**
872 **represent increased q_c required in models and negative biases mean decreased q_c. The**
873 **average percentages of adjustments for different equivalent sizes are shown in panel (c)**
874 **and note that the percentages in the vertical axis are negative.**

875

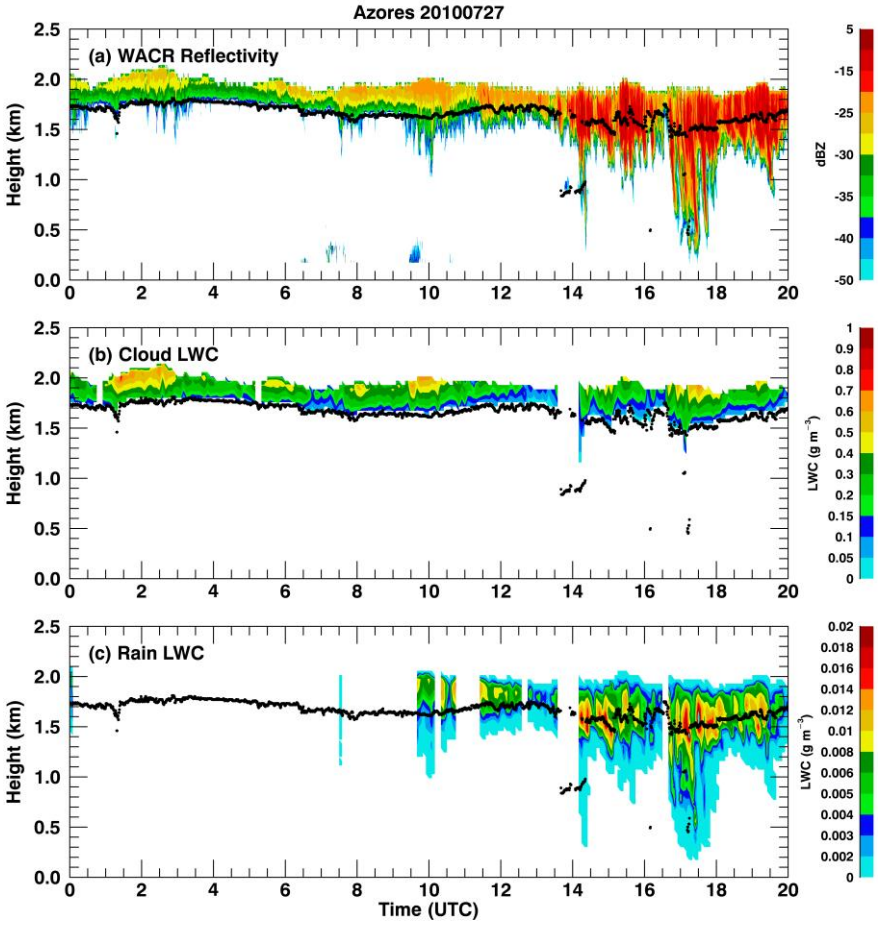

Figure A1. Joint retrieval of cloud and rain liquid water content (CLWC and RLWC) for the same case as in Figure 1. (a) WACR reflectivity, (b) CLWC, and (c) RLWC. The black dots represent cloud base height. Blank gaps are due to the data from one or more observations are not available or reliable. For example, the gap before 14 UTC is due to multiple cloud layers whereas we only focus on single layer cloud.